PIV measurement study on flow around circular cylinders with low aspect ratio piercing the free surface

Conference Paper · June 2018

CITATIONS
0

READS
11

6 authors, including:

Keigo Sakata
The University of Tokyo
2 PUBLICATIONS **0** CITATIONS
SEE PROFILE

Rodolfo Trentin Gonçalves
The University of Tokyo
93 PUBLICATIONS **453** CITATIONS
SEE PROFILE

Gustavo R S Assi
University of São Paulo
51 PUBLICATIONS **457** CITATIONS
SEE PROFILE

Hideyuki Suzuki
The University of Tokyo
106 PUBLICATIONS **288** CITATIONS
SEE PROFILE

Proceedings of the Twenty-eighth (2018) International Ocean and Polar Engineering Conference **www.isope.org**
Sapporo, Japan, June 10-15, 2018

ISBN 978-1-880653-87-6; ISSN 1098-6189

PIV measurement study on flow around circular cylinders with low aspect ratio piercing the free surface

Keigo Sakata[1], Murilo M. Cicolin[2], Rodolfo T. Gonçalves[1],
Shinichiro Hirabayashi[1], Gustavo R. S. Assi[3], Hideyuki Suzuki[1]

1 Department of ocean technology, policy, and environment, Graduate school of University of Tokyo, Kashiwa-shi, Chiba, Japan

2 Department of Mechanical Engineering, Escola Politécnica, University of São Paulo, São Paulo, SP, Brazil

3 Department of Naval Architecture and Ocean Engineering, Escola Politécnica, University of São Paulo, São Paulo, SP, Brazil

ABSTRACT

PIV measurements were carried out in a recirculating water channel at the Reynolds number of 43,000 to understand the three-dimensional flow structures around the free end of the cylinders with low aspect ratio piercing the free surface. Flow fields at different vertical and horizontal planes were presented for two aspect ratios, namely 2.0 and 0.5. The results showed the core of the longitudinal recirculation region (bubbles) varied at different planes for aspect ratio 2.0 and did not vary for aspect ratio 0.5. The difference of vortices showing up between aspect ratio 2.0 and aspect ratio 0.5 was also presented.

KEY WORDS: PIV; flow around circular cylinder; free-surface piercing cylinder; free-end effects; vortex; low aspect ratio.

NOMENCLATURE

D	cylinder diameter
L	submerged cylinder length
L/D	aspect ratio
U	uniform flow velocity
ν	coefficient of kinematic viscosity
Re	Reynolds number ($\mathrm{Re} = \frac{UD}{\nu}$)
Vx	streamwise velocity
Vy	transverse velocity
Vz	vertical velocity
Mean V	time-averaged mean velocity
RMS V	root-mean-square component velocity
$\omega_x D/U$	non-dimensionalized mean streamwise component of vorticity vector ($\omega_x = \frac{\partial V_z}{\partial y} - \frac{\partial V_y}{\partial z}$)
$\omega_y D/U$	non-dimensionalized mean transverse component of vorticity vector ($\omega_y = \frac{\partial V_x}{\partial z} - \frac{\partial V_z}{\partial x}$)
$\omega_z D/U$	non-dimensionalized mean vertical component of vorticity vector ($\omega_z = \frac{\partial V_y}{\partial x} - \frac{\partial V_x}{\partial y}$)
$\omega_m D/U$	non-dimensionalized mean magnitude of vorticity vector ($\omega_m = \sqrt{{\omega_x}^2 + {\omega_y}^2 + {\omega_z}^2}$)

INTRODUCTION

Floating offshore wind turbines (FOWTs) are subjected to severe environmental loads due to winds, waves, and currents. Vortex-induced motion (VIM) is the result of the exciting forces by vortex shedding on the hull of a bluff body exposed to currents. VIM results in additional oscillating mooring line tensions and affects mooring lines' fatigue damage severely. Concerning economy, changing mooring lines is not desirable during the service lifetime of FOWT. The mechanism of VIM needs to be clarified to predict the service lifetime of mooring lines and better design the floating unit. The VIM behavior is susceptible in offshore platforms such as a spar, monocolumn, and multi-columns platforms, see examples by Gonçalves *et al.* (2010, 2012c, 2013b, 2018). The main characteristic of these platforms is to present a low aspect ratio (ratio between the draft and the characteristic diameter).

Structures with low aspect ratio are affected by the free-surface and free-end effects. The free-end effect on vortex shedding in the case of circular cylinders has been studied by many authors for the cylinder positioned on the ground plane (fixed on the bottom), see the example by Kawamura *et al.* (1984). Some investigations have considered the flow structure around the low-aspect-ratio and wall-mounted cylinders. Pattenden *et al.* (2005) sketched the flow around cylinders on the ground plane with aspect ratio equal one, and showed that there are some kinds of vortex namely, tip vortex, arch vortex, trailing vortex, and horseshoe vortex. The paper by Sumner (2013) is an excellent review of this theme. On the other hand, the case of the cylinders with low aspect ratio piercing the free surface needs more attention and to be better studied for the offshore scenario. Hence, this experimental study focused on the flow around stationary circular cylinders with low aspect ratio piercing the free surface to understand the free-end effects. There are few works for L/D<1 and piercing the free surface. Gonçalves *et al.* (2015) measure the drag and lift forces and visualized the flow around two horizontal planes and one vertical plane for low aspect ratio cylinders including the free-surface with L/D=2.0, 1.0, 0.5, 0.3 by PIV. The present study visualized eleven vertical planes for cylinders including the free-surface with L/D=2.0 and 0.5 by PIV and tried to complement this previous work.

The goal of this study is to understand the flow and 3D structures around the cylinders with low aspect ratio.

EXPERIMENTAL SETUP

The experiments were carried out in a recirculating water channel at the NDF – Fluid & Dynamics Research Group Laboratory facility of USP – University of Sao Paulo, Brazil. The scale of the test section is 7500x700x700mm, and the flow has low levels of turbulence (less than 2%). Further details concerning the water channel can be found in Assi *et al.* (2005).

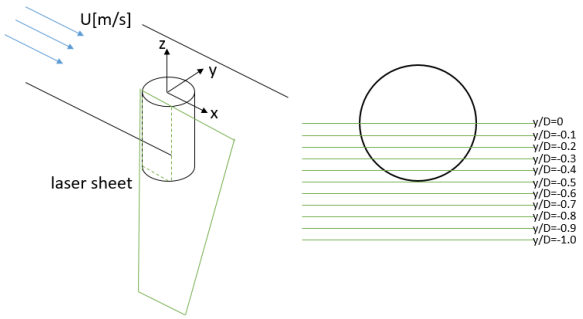

Fig 1.1. Schematic diagram of PIV measurement and laser positions.

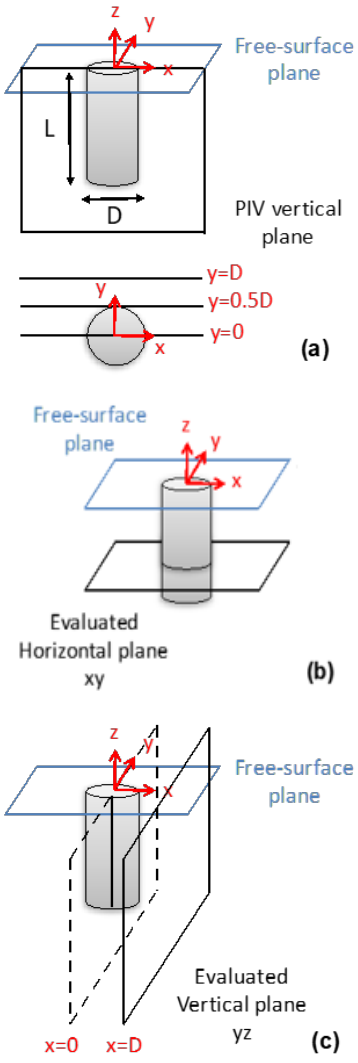

Fig 1.2. (a) PIV measured plane $\boldsymbol{xz}$; (b) evaluated horizontal plane $\boldsymbol{xy}$; (c) evaluated vertical plane $\boldsymbol{yz}$.

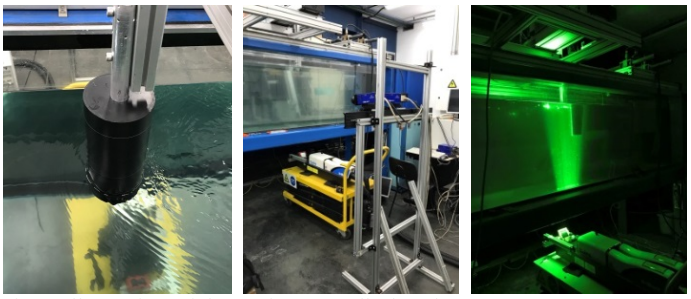

Fig 2. Illustration of the stationary cylinder, the PIV measurement system and the PIV measurement in the vertical plane

Two-dimensional stereo PIV was used aiming at quantifying the flow around the cylinder. 345 snapshots were acquired at a 15Hz sample frequency. Further details regarding the PIV facility can be found in Korkischko & Meneghini (2011).

Stereo PIV measurements (velocity components in 3 directions) were carried out in a recirculating water channel at the Reynolds number of 43,000 to understand the 3D formations around the free end of the cylinders. Two different aspect ratios were tested namely, $AR = L/D = 0.5$ and 2.0 (where L is the submerged length of the cylinder and D is the diameter of the cylinder). Each case was 'sliced' vertically by $D/10$ to reveal the detailed 3D flow structure from the centerline of the cylinder until $D/2$ besides the cylinder. The number of slices was 11 for each aspect ratio, and at least half diameter below the free end and around the cylinder was measured to comprise all the volume around each cylinder case. The composition of the several planes allowed to visualize the 3D flow structures.

Fig.1.1 shows the schematic diagram of PIV measurement. Eleven different vertical planes xz were measured. The vertical planes acquired were spaced 0.1 diameters each other from the cylinder center plane at $y/D = 0$ to $|y/D| = 1$. Due to the stereo characteristic of the measurements, the velocities in the vertical plane xz and horizontal planes xy and yz can be evaluated (Fig.1.2). The model was made of PVC – polyvinyl chloride with external diameter $D = 125\,\text{mm}$. See details about the PIV setup and measurements in Fig.2.

RESULTS & DISCUSSION

Time-averaged fields & root mean square fields

(a) Vertical planes xz

Selected flow fields for Re=43000, $L/D = 2.0$ and $L/D = 0.5$ are presented in Fig.3-Fig.9. In these figures, both the mean velocity field and the mean vorticity field are made dimensionless with the uniform flow velocity $U = 0.344\text{m/s}$ and the cylinder diameter $D = 0.125\text{mm}$. The white square means the position of the cylinder submerged and the top line is the free-surface. In this PIV measurement, near the free surface was not able to be measured due to the reflection of water.

Fig. 3 shows the time-averaged streamlines and contours of mean velocity component Vx/U in different vertical planes xz for $L/D = 2.0$. At $|y/D| < 0.6$, recirculation flow from the bottom of the cylinder can be observed. The transition of the recirculation core of each vertical plane is found. The other recirculation under the cylinder ($|x/D| < 0.5$ and $z/D < -2.0$) disappears at $|y/D| > 0.4$. At $|y/D| > 0.6$, the regions of which region are less susceptible by the cylinder, the stream direction is almost the same as that of uniform flow.

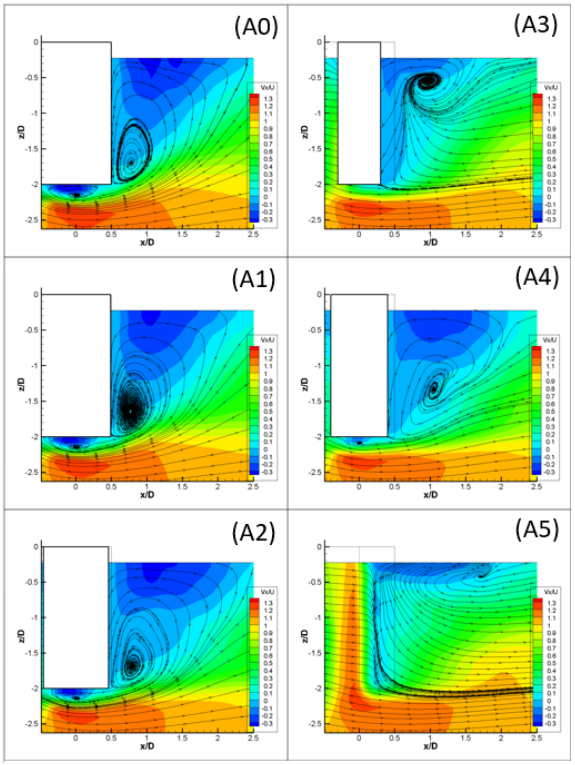

Fig 3. Time-averaged streamlines and contours of mean velocity component Vx/U in the vertical planes xz for $L/D = 2.0$ at Re=43000: (A0) $y/D = 0$, (A1) $|y/D| = 0.1$, (A2) $|y/D| = 0.2$, (A3) $|y/D| = 0.3$, (A4) $|y/D| = 0.4$, (A5) $|y/D| = 0.5$.

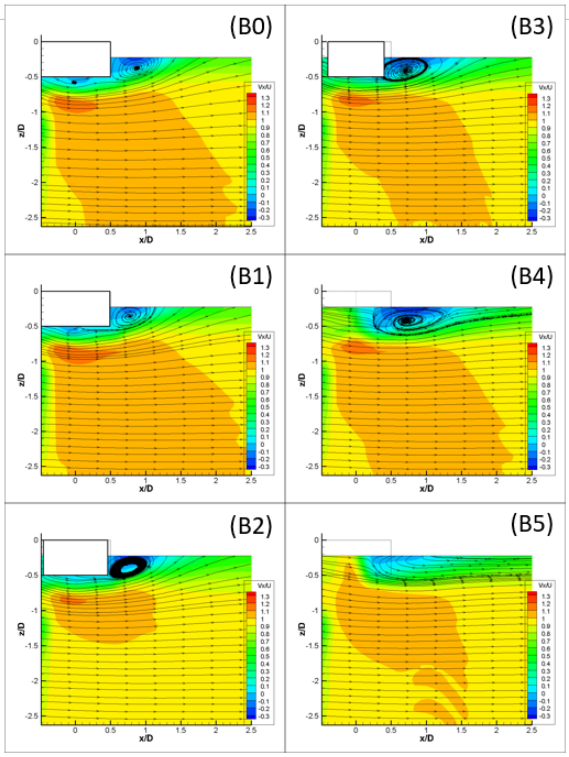

Fig 4. Time-averaged streamlines and contours of mean velocity component Vx/U in the vertical planes xz for $L/D = 0.5$ at Re=43000: (B0) $y/D = 0$, (B1) $y/D = -0.1$, (B2) $y/D = -0.2$, (B3) $y/D = -0.3$, (B4) $y/D = -0.4$, (B5) $y/D = -0.5$.

Fig.4 shows the time-averaged streamlines and contours of mean velocity component Vx/U in the vertical plane xz for $L/D = 0.5$. Unlike the case with the aspect ratio of 2.0, recirculation flow from the bottom of the cylinder can be observed only in $|y/D| < 0.4$. The recirculation core of each vertical plane did not change at different planes. Positions of the core of longitudinal recirculation region behind the cylinder for $L/D = 2.0$ and $L/D = 0.5$ are presented in Table1 and Fig.5. The same type of comparison in the y/D=0 was presented by Palau-Salvador *et al.* (2010) for $L/D = 2.5$ and 5.0, and by Gonçalves *et al.* (2015) for L/D =0.3, 0.5,1.0, and 2.0. The other recirculation under the cylinder ($|x/D| < 0.5$ and $z/D < -0.5$) disappears at $|y/D| > 0.2$.

Table 1. Positions of the core of the longitudinal recirculation region behind the cylinders with different aspect ratios.

L/D	$\|y/D\|$	x/D	$\|z/D\|$	$\|z/L\|$
2	0.0	0.75	1.75	0.875
2	0.1	0.75	1.75	0.875
2	0.3	0.75	1.75	0.875
2	0.3	1.10	1.25	0.625
2	0.4	0.90	0.55	0.275
2	0.5	1.75	0.40	0.200
2	0.6	1.10	0.25	0.125
0.5	0.0	0.80	0.35	0.700
0.5	0.1	0.80	0.35	0.700
0.5	0.2	0.80	0.40	0.800
0.5	0.3	0.75	0.40	0.800
0.5	0.4	0.70	0.40	0.800

Fig 6. shows contours of the mean transverse vorticity in the vertical planes xz. The vorticity was calculated by the following equation, see Fig.7 for details.

$$\omega_y \; at \; (i,j) = \frac{V_{x_{i,j-1}} - V_{x_{i,j+1}}}{\Delta Z} - \frac{V_{z_{i+1,j}} - V_{z_{i-1,j}}}{\Delta X}$$

Vorticities in other two directions were calculated in the same way. Both cases confirmed the vortex from the bottom at $|y/D| < 0.5$. Although Gonçalves *et al.* (2015) presented the same cases as $y/D = 0$, the value of this study is correct. The vortex from the bottom is gradually stretched out in the streamwise direction away from the centerline. On the other hand, at $|y/D| > 0.5$, the vortex comes from the side of the cylinder. For $L/D = 2.0$, the vortex shedding from the side is dragged to z-direction because the streamline direction is like Fig.3.

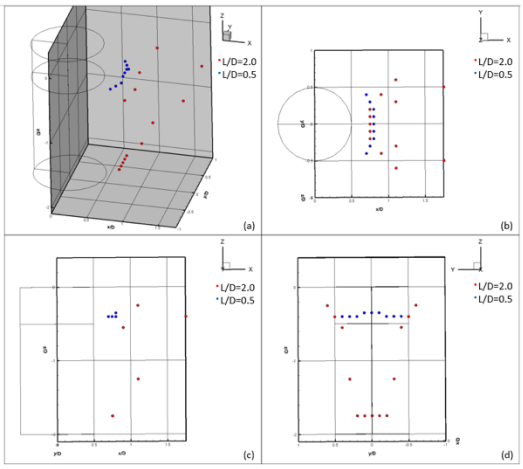

Fig 5. Positions of the core of the longitudinal recirculation region behind the cylinders for Re=43000, (a) 3D (b) top view (c) side view (d)front view.

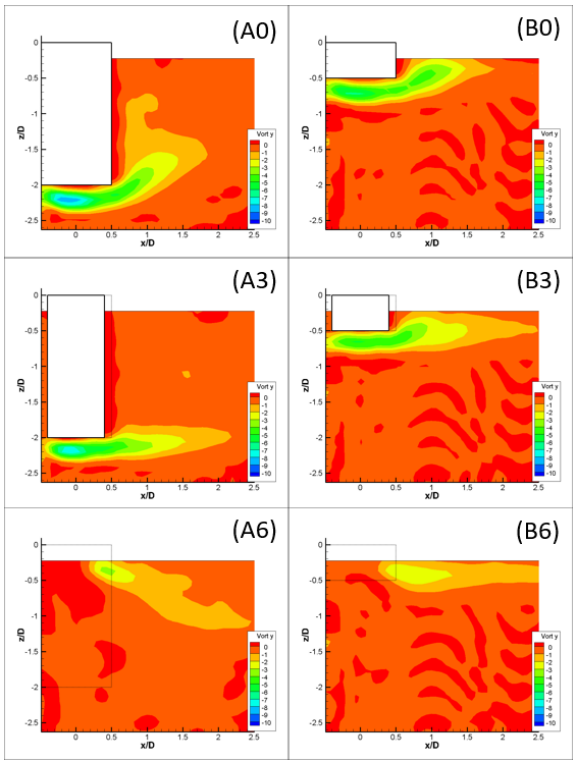

Fig 6. Contours of mean transverse vorticity $\omega_y D/U$ in the vertical planes xz for Re=43000, $L/D = 2.0$: (A0) $y/D = 0$, (A3) $y/D = -0.3$, (A6) $y/D = -0.6$, $L/D = 0.5$: (B0) $y/D = 0$, (B3) $y/D = -0.3$, (B6) $y/D = -0.6$.

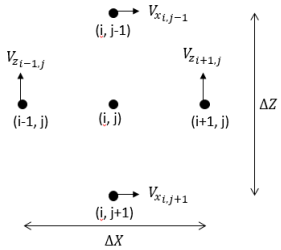

Fig 7. Vorticity calculation model

Fig.8 and Fig.9 show contours of root mean square of streamwise and transverse velocity fluctuations RMS Vx/U, RMS Vz/U in the vertical planes xz. Each velocity fluctuation was calculated as root mean square of the deviation from time-averaged velocity. RMS Vx/U behind the cylinder for $L/D = 2.0$ becomes larger away from the centerline. On the other hand, RMS Vz/U behind the cylinder becomes smaller away from the centerline. This is because, near the centerline, the vortex from the bottom is preeminent, but away from the centerline, the streamwise velocity is strengthened by the separation from the side of the cylinder. As Palau-Salvador *et al.* (2010) pointed out for $L/D = 2.5$, the elevated RMS Vx/U behind the cylinder at $|y/D| = 0$ may be caused by an energy transfer from the much larger RMS Vz/U. This explanation is also true of the case at $|y/D| = 0.6$. The elevated RMS Vz/U behind the cylinder at $|y/D| = 0$ may be caused by an energy transfer from the much larger RMS Vx/U. The high-velocity fluctuations behind the cylinder are not aligned with the shear layer bordering the longitudinal recirculation region. Comparing with two aspect ratio cases in $|y/D| = 0.6$, the value of $L/D = 2.0$ behind the cylinder was larger than that of $L/D = 0.5$ because of the Karman vortex shedding. For $L/D = 0.5$, at $|y/D| = 0$ and 0.3, the high-velocity fluctuations behind the cylinder are

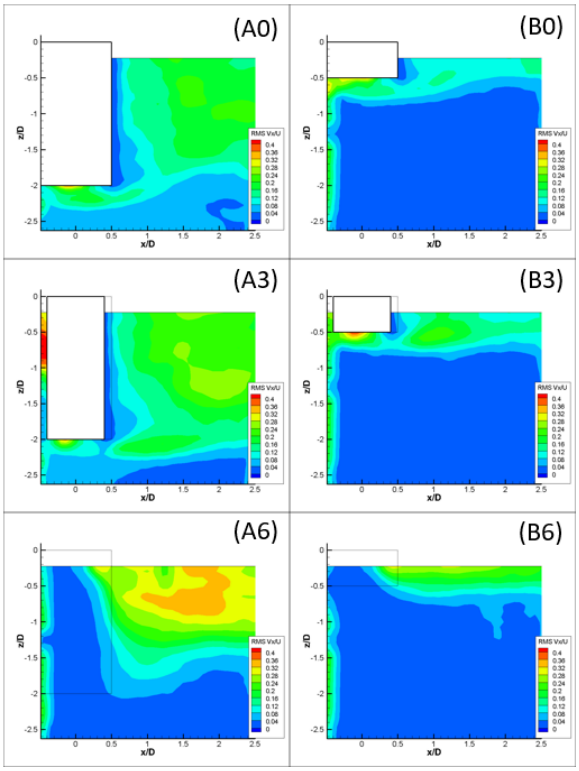

Fig 8. Contours of root mean square of streamwise fluctuations RMS Vx/U in the vertical planes xz for Re=43000, $L/D = 2.0$: (A0) $y/D = 0$, (A3) $y/D = -0.3$, (A6) $y/D = -0.6$, $L/D = 0.5$: (B0) $y/D = 0$, (B3) $y/D = -0.3$, (B6) $y/D = -0.6$.

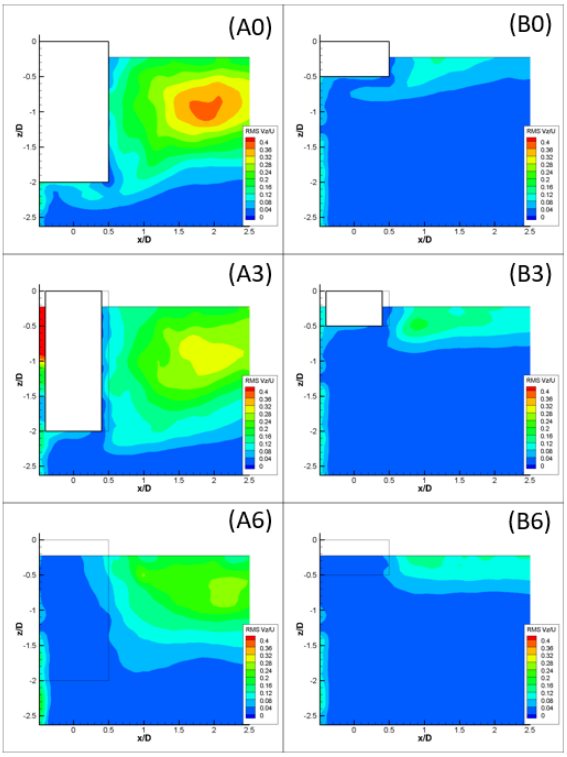

Fig 9. Contours of root mean square of vertical fluctuations RMS Vz/U in the vertical planes xz for Re=43000, $L/D = 2.0$: (A0) $y/D = 0$, (A3) $y/D = -0.3$, (A6) $y/D = -0.6$, $L/D = 0.5$: (B0) $y/D = 0$, (B3) $y/D = -0.3$, (B6) $y/D = -0.6$.

aligned with the shear layer bordering the longitudinal recirculation region. Unlike the cases of $L/D = 2.0$, the velocity fluctuations behind the cylinder of $|y/D| = 0.3$ are higher than that of $|y/D| = 0$. At $|y/D| = 0.6$, the high-velocity fluctuations behind the cylinder are aligned with the separation from the side of the cylinder.

(b) Horizontal planes xy

Fig.10 shows contours of the mean vertical vorticity in the vertical planes xz at different horizontal slices. Separation can be confirmed vertically from $z/D = -0.23$ to the end of each cylinder.

(c) Vertical planes yz

Fig.11 shows contours of the mean vertical vorticity in the vertical planes yz at $x/D = 0$. The vorticity below the bottom of the cylinder means trailing vortex. However, it is hard to detect the tip vortex from the corner of the bottom.

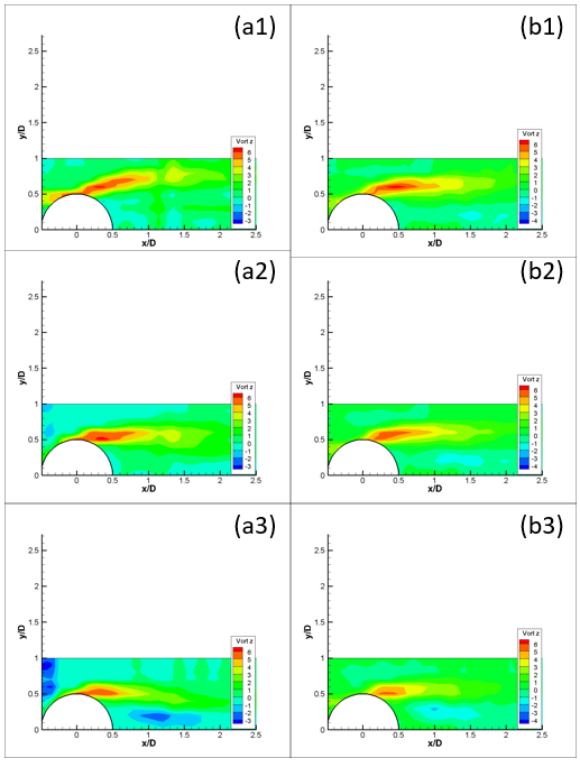

Fig 10. Contours of mean vertical vorticity $\omega_z D/U$ in the horizontal planes xy at Re=43000, $L/D = 2.0$:(a1) $z/D = -0.23$,(a2) $z/D = -1.0$, (a3) $z/D = -2.0$, $L/D = 0.5$:(b1) $z/D = -0.23$, (b2) $z/D = -0.37$, (b3) $z/D = -0.51$.

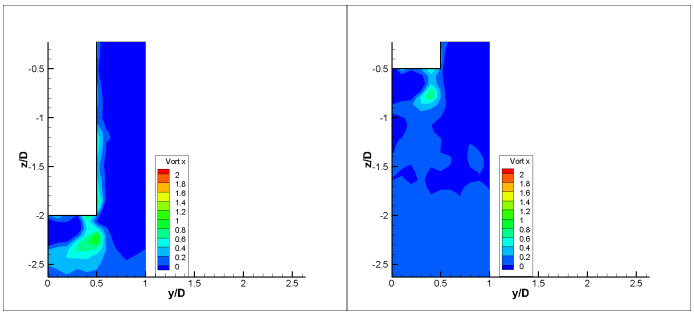

Fig 11. Contours of mean vertical vorticity $\omega_x D/U$ in the horizontal planes yz ($x/D = 0$) at Re=43000 for $L/D = 2.0$ and $L/D = 0.5$.

3D flow structures

Since each vertical PIV plane has three velocity components, three-dimensional flow fields can be constructed. However, each plane was measured independently, and three-dimensional flow fields are time-averaged fields.

Fig.12 shows iso-surfaces of non-dimensionalized mean vorticity magnitude at 3.5 for $L/D = 2.0$. Inside the green color area, the dimensionless vorticity is bigger than 3.5. Fig.13 shows iso-surfaces of non-dimensionalized mean vorticity magnitude at 3.5 for $L/D = 0.5$. Inside the yellow, green color area, the dimensionless vorticity is higher than 3.5. For both aspect ratio cases, separation and the arch-type vortex structure were confirmed.

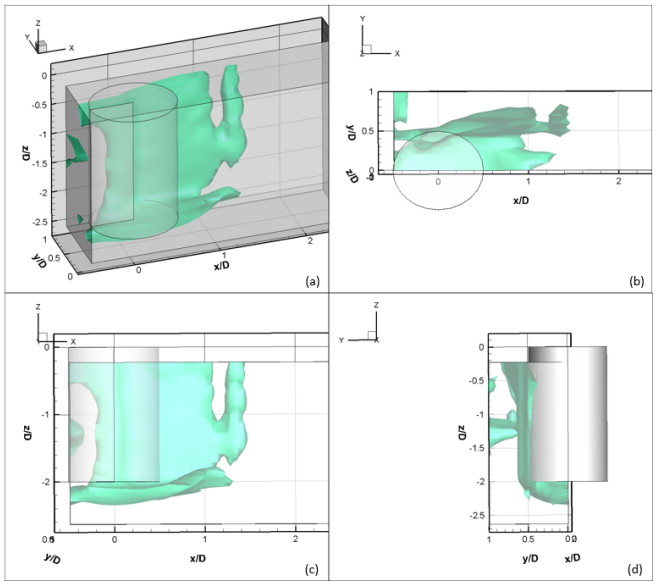

Fig 12. Iso-surfaces of non-dimensionalized mean magnitude of vorticity vector at 3.5 for Re=43000, $L/D = 2.0$: (a) 3D (b) top view (c) side view and (d) front view.

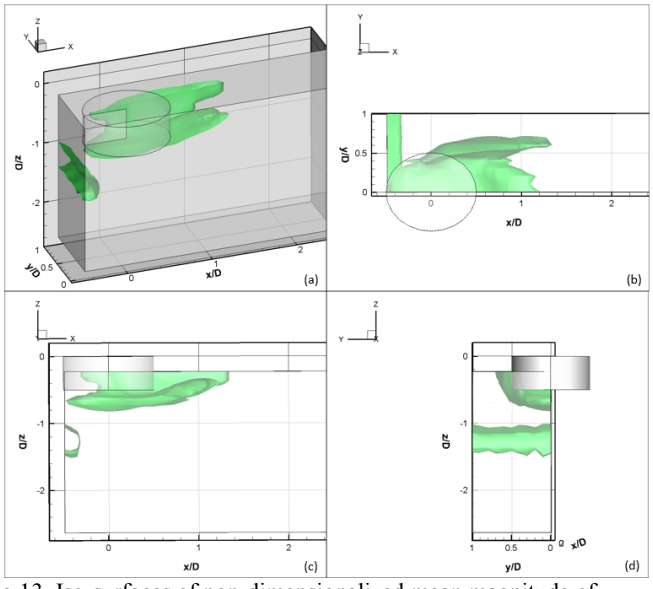

Fig 13. Iso-surfaces of non-dimensionalized mean magnitude of vorticity vector at 3.5 for Re=43000, $L/D = 0.5$: (a) 3D (b) top view (c) side view and (d) front view.

Fig.14 show iso-surfaces of non-dimensionalized mean streamwise vorticity at 1 for (a) $L/D = 2.0$ and at 0.6 for (b) $L/D = 0.5$. Inside the blue color area, the dimensionless vorticity is bigger than each value. This streamwise vortex is supposed to be the trailing vortex, and it is remarkable for $L/D = 2.0$.

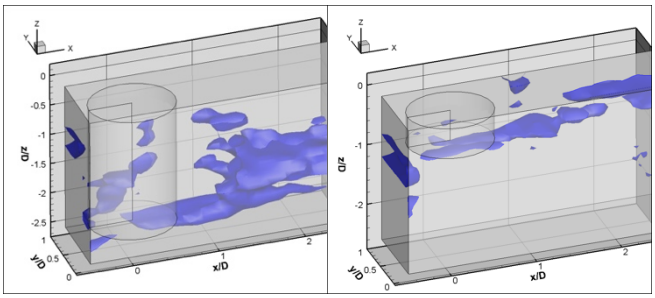

Fig 14. Iso-surfaces of non-dimensionalized mean streamwise vorticity at 1 for (a) $L/D = 2.0$ and at 0.6 for (b) $L/D = 0.5$.

Fast Fourier Transformation analysis

To better understand the dynamics of the wake, FFT analysis was conducted. Vortex shedding frequency cannot be evaluated correctly only by this PIV measurement. Instead of evaluating time series vorticity directly, streamwise velocity is processed by FFT, and 'f' is defined as the frequency.

Fig.15 shows the power spectrum densities of the streamwise velocity of the non-dimensionalized streamwise velocity at different z/D positions as a function of non-dimensionalized frequency fD/U at $x/D = 2.5$, $|y/D| = 0.6$, for (a) $L/D = 2.0$ and (b) $L/D = 0.5$. This frequency can be regarded as that of von Karman vortex shedding from the side of the cylinder.

The case of $L/D = 2.0$ has a strong peak around $fD/U = 0.13$ at $z/D > -0.6$, which frequency is supposed to correspond to the von Karman vortex shedding from the side. And the strong peak gradually disappears alongside $z/D < -0.6$. This is because of the free-end effect. On the other hand, the case of $L/D = 0.5$ has a very weak peak around $fD/U = 0.18$ at $z/D > -0.5$. This suggests that for $L/D = 0.5$, the von Karman vortex shedding cannot be confirmed clearly, affected by the flow from the free end.

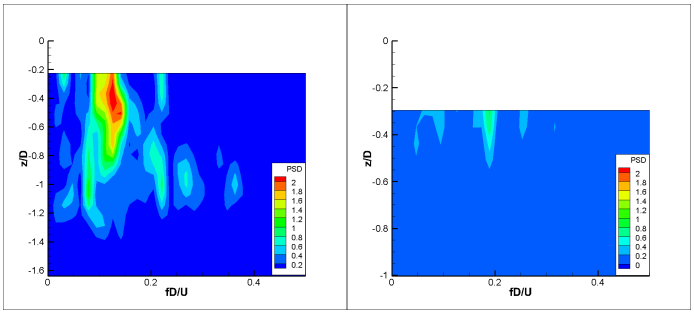

Fig 15. PSD of the non-dimensionalized streamwise velocity as a function of fD/U at $x/D = 2.5$, $|y/D| = 0.6$, (a) $L/D = 2.0$, (b) $L/D = 0.5$

Fig.16 shows the power spectrum densities of the streamwise velocity of the non-dimensionalized streamwise velocity at different y/D positions as a function of non-dimensionalized frequency fD/U at $x/D = 2.5$, $z/D = -0.3$, for (a) $L/D = 2.0$ and (b) $L/D = 0.5$. At $|y/D| > 0.5$, there are strong peaks for $L/D = 2.0$ and weak peaks for $L/D = 0.5$. This means that at $|y/D| > 0.5$, there is the von Karman vortex shedding for $L/D = 2.0$, but it cannot be concluded that there is also the von Karman vortex shedding for $L/D = 0.5$.

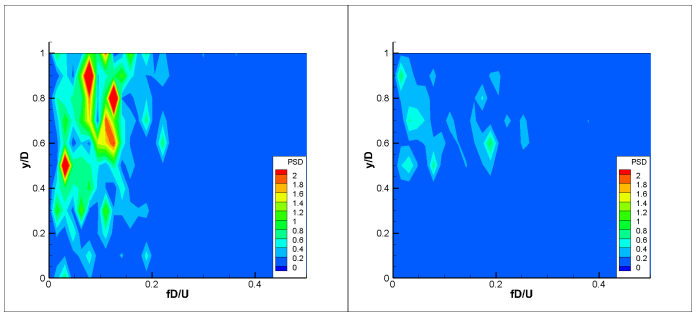

Fig 16. PSD of the non-dimensionalized streamwise velocity as a function of fD/U at $x/D = 2.5$, $z/D = -0.3$, (a) $L/D = 2.0$, (b) $L/D = 0.5$.

CONCLUSIONS

Particle image velocimetry was used to investigate the flow around the free end of the cylinders with low aspect ratio piercing the free surface. The flow fields at different vertical and horizontal planes were analyzed for $L/D = 2.0$ and 0.5. It was newly found that the core of the longitudinal recirculation region (bubbles) varied at different planes for $L/D = 2.0$ and did not vary for $L/D = 0.5$. Moreover, the trailing vortex, separation and the arch-type vortex structure were confirmed for both aspect ratios. For $L/D = 2.0$, the von Karman vortex shedding was confirmed. For $L/D = 0.5$, the von Karman vortex is suppressed by the free-end effect and does not appear clearly. These were validated by FFT. Horseshoe vortex and tip vortex, which are characteristic for cylinders on the ground plane were not confirmed for both cases.
In this PIV measurement, near the free surface was not measured and the free-surface effect cannot be evaluated correctly. Therefore, to reveal the minute characteristic including free-surface, another experiment is needed. And another idea is to do POD (Proper Orthogonal Decomposition) analysis to extract the feature of flow fields. These are left to our future work.

ACKNOWLEDGEMENTS

The authors would like to acknowledge the Japan Society of Naval Architects and Ocean Engineers (JASNAOE) for the financial support for the occasion of the PIV measurements.

REFERENCES

Assi, G.R.S., Meneghini, J.R., Aranha, J.A., Coleto, W.G.P. (2005) "Design, assembling and verification of a circulating water channel facility for fluid dynamics experiments," *Proc. of the ABCM 18th International Congress of Mechanical Engineering*, COBEM. Ouro Preto, Minas Gerais, Brazil.

Fujarra, A.L.C., Rosetti, G.F., Wilde, J., and Gonçalves, R.T. (2012) "State-of-art on vortex-induced motion: A comprehensive survey after more than one decade of experimental investigation," *Proc. of the ASME 31st International Conference on Ocean, Offshore and Arctic Engineering*, OMAE2012-83561, Rio de Janeiro, Brazil, 2012.

Kawamura,T., Hiwada,M., Hibino,T., Mabuchi,I., Kumada,M. (1984) "Flow around a finite circular cylinder on a flat plate," *Bulletin of the Japan Society of Mechanical Engineers*, 27, pp. 2142–2151.

Korkischko, I., Meneghini, J.R. (2011) "Volumetric reconstruction of the mean flow around circular cylinders fitted with strakes," *Experiments in Fluids*, 51, pp. 1109–1122.

Iungo, G.V., Pii, L.M., Buresti, G. (2012) "Experimental investigation

on the aerodynamic loads and wake flow features of a low aspect-ratio circular cylinder," *Journal of Fluids and Structures*, 28, pp. 279–291.
Gonçalves, R.T., Rosetti, G.F., Fujarra, A.L.C., Nishimoto, K. (2010) "Mitigation of vortex-induced motion (VIM) on a monocolumn platform: forces and movements," *J. Offshore Mech. Arctic Eng.*, 132, pp. 041102-1-16.
Gonçalves, R.T., Rosetti, G.F., Fujarra, A.L.C., Oliveira, A.C. (2012) "Experimental study on vortex-induced motions of a semi-submersible platform with four square columns, Part I: effects of current incidence angle and hull appendages," *Ocean Eng.*, 54, pp. 150–169.
Gonçalves, R.T., Rosetti, G.F., Fujarra, A.L.C., Oliveira, A.C. (2013) "Experimental study on vortex-induced motions of a semi-submersible platform with four square columns, Part II: effects of surface waves, external damping and draft condition," *Ocean Eng.*, 62, pp. 10–24.
Gonçalves, R.T., Franzini, G.F., Rosetti, G.F., Meneghini, J.R., Fujarra, A.L.C. (2015) "Flow around circular cylinders with very low aspect ratio," *J. Fluid Struct.*, 54, pp. 122–141.
Gonçalves, R.T., Fujarra, A.L.C., Rosetti, G.F., Kogishi, A.M., Koop, A. (2018) "Experimental study of the column shape and the roughness effects on the vortex-induced motions of deep-draft semi-submersible platforms," *Ocean Eng.*, 149, pp. 127–141.
Okamoto, T., Yagita, M. (1973) "The experimental investigation on the flow past a circular cylinder of finite length placed normal to the plane surface in a uniform stream," *Bulletin of the Japan Society of Mechanical Engineers*, 16, pp. 805-814.
Pattenden, R.J., Turnock, S.R., Zhang, X. (2005) "Measurements of the flow over a low-aspect-ratio cylinder mounted on a ground plane," *Experiments in Fluids*, 39, pp. 10–21.
Palau-Salvador, G., Stoesser, T., Fröhlich, J., Kappler, M., Rodi, W. (2010) "Large eddy simulations and experiments of flow around finite-height cylinders," *Flow, Turbulence and Combustion*, 84, pp. 239–275.
Sumer, D. (2013) "Flow above the free end of a surface-mounted finite-height circular cylinder: a review," *J. Fluid Struct*. 43, pp. 41–63.